




Cite this: *New J. Chem.*, 2023, 47, 11615

# FeS<sub>2</sub>-based aerogel as a flexible low-cost substrate for rapid SERS detection of histamine in biofluids†

Anjali Sreekumar, Lignesh Durai, Minu Thomas and Sushmee Badhulika \*

Histamine is an organic nitrogenous compound released from mast cells, often as part of an instant immune response. Life-threatening anaphylaxis can occur with significant histamine intolerance, which is also referred to as histaminosis caused by overproduction of histamine in the body. Herein, we demonstrate the synthesis of FeS<sub>2</sub>-incorporated rGO aerogel (FeS<sub>2</sub>-AG) by lyophilization, as an active SERS substrate for the detection of histamine in blood serum. The morphological characterization revealed the nanoflower structure of FeS<sub>2</sub> and uniform porosity of the aerogel, in which the nanoflower structure of FeS<sub>2</sub> was homogeneously distributed on the surface of the porous aerogel. The cubic structure of FeS<sub>2</sub> nanoflowers was revealed by X-ray diffraction and Fourier transform infrared spectroscopy demonstrated the characteristic peak at ~1176 cm<sup>-1</sup> which is related to pyrite surface chemistry of FeS<sub>2</sub> nanoparticles. The as-fabricated sensor exhibited an enhancement factor of 1.61 × 10<sup>7</sup> with a limit of detection of 0.08 ng mL<sup>-1</sup>. The substrate exhibited a good selectivity and linear range of detection towards histamine in the presence of 2-fold concentration of ascorbic acid, glucose, urea, and uric acid. This excellent performance of the sensor can be ascribed to the chemical enhancement occurring via the interaction of oxy functional groups of aerogel and multiple coordination sites (ferrous ions (Fe<sup>2+</sup>)) of FeS<sub>2</sub> with histamine molecules causing reconstruction of the band gap. This newly formed energy band further leads to the occurrence of the Raman resonance effect, providing an enhancement in the SERS signal over that of the Raman signal obtained from bulk histamine. The sensor showed good recovery percentage of 97.25% from real samples, highlighting the efficiency of the as-fabricated sensor towards histamine detection.

Received 15th April 2023,  
Accepted 22nd May 2023

DOI: 10.1039/d3nj01736b

rs.c.li/njc

## 1. Introduction

Histamine is a ubiquitous biogenic amine associated with local immune responses regulating a plethora of pathophysiological functions in the gut and serving as a neurotransmitter for the spinal cord, brain, and uterus.<sup>1</sup> Histamines start the process that hustles allergens out from the body and skin and are thus associated with common allergic responses and symptoms. This preserved autacid is distributed widely throughout the body and is found in the tissues of most vertebrates, in basophils and mast cells.<sup>2</sup> Histamine intolerance, a non-immune reaction, is a type of food intolerance which is caused by accumulation and ingestion of histamine, causing an increase in exogenous histamine, resulting in an increase in its concentration followed by a series of discomforts in the body such as itching, stress,

flushing, aggression, diarrhoea, vomiting and headache. Histamine exists in “Nτ-H” and “Nπ-H” tautomeric forms in water with a chemical structure including two basic centres of an aliphatic amino group and the other with a possible nitrogen in the imidazole without a proton.<sup>3</sup> Moreover, there are some foods high in histamine that can trigger inflammatory reactions causing intoxication. The plasma concentrations of histamine are in the 0.3 to 1.0 ng mL<sup>-1</sup> range and any increase in concentration may exacerbate the allergic symptoms. Thus, accurate quantification and rapid measurement of histamine levels are therefore essential with scientific implications for clinical diagnostics as well as food safety.<sup>4</sup>

Several approaches have been developed for the sensing of histamine concentration in the body. The classical analytical methods such as capillary electrophoresis, liquid chromatography, and electrochemical-based methods provide the advantages of enrichment and separation. Moreover, these take a longer operation period and have limited spatial resolution. It is therefore necessary to develop simple, rapid, and more sensitive analytical strategies to detect histamines.<sup>5,6</sup> Recently, low-cost,

Department of Electrical Engineering, Indian Institute of Technology, Hyderabad 502285, India. E-mail: sbadh@iith.ac.in; Tel: +040-23016467

† Electronic supplementary information (ESI) available. See DOI: <https://doi.org/10.1039/d3nj01736b>

surface-enhanced Raman scattering (SERS) sensing platforms have been intensively studied for chemical and biological analysis at high throughput. Due to high sensitivity and molecular specificity, SERS is among the most promising analytical techniques for detecting trace amounts of molecules. A metal coordination-induced SERS nanoprobe has been reported<sup>7</sup> for sensitive and selective detection of histamine in serum using histamine-Ni<sup>2+</sup> complex capturing histamine molecules near hot spots of material owing the amplification of Raman signals.

In SERS, incorporating an analyte onto a plasmonic substrate significantly enhances the Raman scattering signals owing to the surface plasmon resonance of the material which can then be used for structural identification or quantitative analysis. A high electromagnetic field near the plasmonic substrates is largely responsible for the notable Raman scattering enhancements of the analytes.<sup>8</sup> However, plasmonic substrates are highly expensive, of low abundance, and toxic, while earth-abundant metals can offer unique advantages that address the disadvantages of precious metals.<sup>9</sup>

The transition-metal dichalcogenides are well suited for SERS-based detection as they provide atomically flat surfaces facilitating homogenous distribution of analyte. Surface functionalization, and/or structural engineering and defect engineering, provides the advantage of controllability over band structure.<sup>10</sup> Nano-sized iron sulphides have attracted intense research interest due to the variety of their types, structures, and physicochemical properties.<sup>11</sup> The electronic conductivity of iron sulphide is greater compared to iron oxide owing to the smaller band gap of iron sulphide and more appropriate electron transfer. Therefore, iron sulphide nanomaterials are anticipated to display multiple functionalities.<sup>12</sup>

As high-performance sensing materials in gas sensors, biosensors, strain and pressure sensors, *etc.*, aerogels have attracted a lot of attention. With a large specific surface area, an aerogel retains its basic properties while allowing its compositions and structures to be easily modified to obtain ideal SERS substrate materials. Notably, the highly electronegative oxygen-containing atoms in graphene oxide (GO) can generate a strong local electric field on the adsorbed surface, which is beneficial for SERS performance.<sup>13,14</sup> In particular, incorporating SERS materials into 3D aerogels provides a combination of the material's intrinsic qualities with the material's large surface area and high porosity, resulting in new possibilities for the creation of 3D SERS substrates.<sup>15</sup>

In this study, we fabricated FeS<sub>2</sub> aerogel (FeS<sub>2</sub>-AG) as a sensitive SERS substrate for the detection of histamine in simulated human blood serum. The FeS<sub>2</sub> aerogel exhibited outstanding SERS properties through chemical enhancement provided by the charge transfer resonance mechanism of FeS<sub>2</sub> nanoflower structure with the histamine molecule. The energy band reconstruction at the interface of metallic sites of FeS<sub>2</sub>-AG and histamine molecules makes the energy of the newly formed band closer to the excited laser photon energy. These energy bands between the excited laser and the molecule interface lead to a Raman resonance effect. According to the authors' knowledge, this is the first study into the use of FeS<sub>2</sub>-AG as an active

substrate for SERS-based histamine detection in biofluids. This exceptional performance of FeS<sub>2</sub>-AG stands as a testament to its great potential as a SERS platform.

## 2. Experimental section

### 2.1. Materials and methods

The chemical reagents sodium thiosulfate  $\geq 99.99\%$  (Na<sub>2</sub>S<sub>2</sub>O<sub>3</sub>), iron(II) chloride 98% (FeCl<sub>2</sub>·5H<sub>2</sub>O), methylene blue  $\geq 95\%$ , polyacrylic acid 99%, and ammonium persulfate 99.99% were obtained from Sigma Aldrich. The DI water used was from a Millipore system and was of 18.2 M $\Omega$  cm resistivity at room temperature. All the chemicals were used without any purification process and were of analytical grade.

### 2.2. Synthesis of FeS<sub>2</sub> nanoflowers

A facile one-pot hydrothermal synthesis technique was employed to prepare FeS<sub>2</sub> nanoflowers. At first, a nutrient solution was prepared by mixing Na<sub>2</sub>S<sub>2</sub>O<sub>3</sub> and FeCl<sub>2</sub> in 30 mL distilled water and stirred continuously for 1 hour yielding a black solution. Then, the black solution was transferred into a 50 mL Teflon-lined autoclave, and further transferred to an oven at 200 °C for 20 hours. The precipitate obtained was centrifuged and washed with DI water and ethanol. The obtained black powder was dried at 70 °C to afford FeS<sub>2</sub> nanoflowers. Fig. 1 depicts the hydrothermal synthesis of FeS<sub>2</sub>.

### 2.3. Synthesis of FeS<sub>2</sub> aerogel

The FeS<sub>2</sub>-based aerogel was prepared using simple two steps of polymerization and hydrothermal reduction process. Briefly, 12.5 mL 1 M HCl and 6.3 mL polyacrylic acid were mixed uniformly with magnetic stirring, and a solution of 25 mg FeS<sub>2</sub> and 25 mg GO in 12.5 mL distilled water was added dropwise. The resultant mixture was stirred under magnetic stirring in an ice bath after sonicating for 0.5 hour. The mixture was left for polymerization reaction for 10 hours in an ice bath after adding 5 mg ammonium persulfate (APS) in 2.5 mL water dropwise. Thereafter, the polymer composites obtained were filtered and washed to be neutral with deionized water, followed by reducing by hydrothermal method at 120 °C for 4 hours by adding 10 mg of L-ascorbic acid. Finally, this solution was transferred into a Petri plate and lyophilized for 24 hours to obtain FeS<sub>2</sub>-AG.

### 2.4. Substrate fabrication and instrumentation

The FeS<sub>2</sub> aerogel with dimensions of 1 cm  $\times$  1 cm was used as a substrate for all the measurements. The measurements were taken by drop-casting different concentrations of histamine from 0.5 to 100 ng mL<sup>-1</sup> onto the substrate. All the measurements were taken using a laser of  $\lambda = 532$  nm and power of 0.32 mW. An objective lens of A  $\times$  50 long distance (LD) was used for analysis.

Scanning electron microscope (SEM), Zeiss Ultra-55 model, was used for morphological characterization studies of the FeS<sub>2</sub> aerogel. The crystallographic study was done using X-ray diffraction (XRD) with Cu-K $\alpha$  ( $\lambda = 1.54$  Å) in a  $2\theta$  range of 10 to 80° using a lineon X'pert PRO X-ray diffractometer. Raman spectroscopy

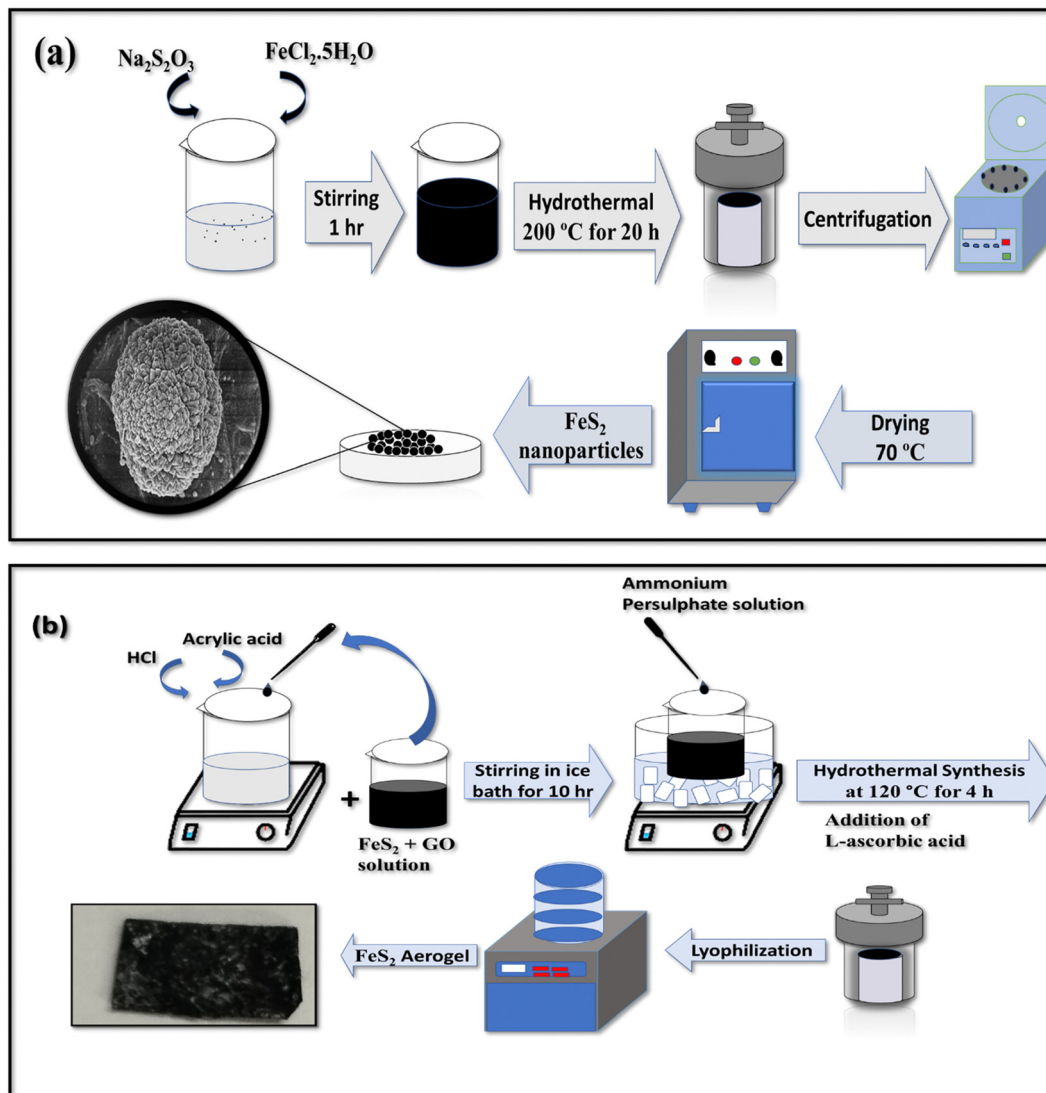


Fig. 1 (a) Synthesis of  $\text{FeS}_2$  nanoflowers. (b)  $\text{FeS}_2$ -based aerogel synthesis by freeze-drying process.

was conducted using a Witech alpha-300 confocal microscope for determining the vibrational bands. All the SERS measurements were done using the same spectrometer with 20 s accumulation time and a laser source of  $\lambda = 532$  nm. Fourier transform infrared (FTIR) spectroscopy with an IR Affinity spectrophotometer ranging from  $400\text{ cm}^{-1}$  to  $4000\text{ cm}^{-1}$  was utilized to study the surface functional groups.

### 3. Results and discussion

#### 3.1. Physiochemical and morphological studies

The morphological properties of the  $\text{FeS}_2$  aerogel were studied from SEM micrographs. Fig. 2(a) shows the SEM image of  $\text{FeS}_2$  nanoflowers with an average size of 85 nm. Fig. 2(b) depicts the low-magnification SEM image of  $\text{FeS}_2$  aerogel and the inset shows the high-magnification image of  $\text{FeS}_2$  aerogel which clearly shows the homogenous distribution of  $\text{FeS}_2$  nanoflowers on the surface of the aerogel. The crystal structure of the as-

synthesized  $\text{FeS}_2$  nanoflowers and  $\text{FeS}_2$  aerogel was studied *via* XRD analysis as depicted in Fig. 1(c). The diffraction peaks were observed at  $2\theta \sim 28^\circ, \sim 32^\circ, \sim 36^\circ, \sim 40^\circ, \sim 47^\circ, \sim 56^\circ, \sim 61^\circ,$  and  $\sim 64^\circ$  which indexed the presence of (111), (200), (210), (211), (220), (222), (230), and (321), whereas for the  $\text{FeS}_2$  aerogel, the diffraction peaks were observed at  $2\theta \sim 21^\circ, \sim 27^\circ,$  and  $\sim 39^\circ$ , which correspond to the crystallographic planes (220), (222), and (313), respectively. Specifically, the peak observed at  $21^\circ$  corresponds to the crystalline structure of GO, while another peak observed at  $27^\circ$  is attributed to the presence of polyvinyl alcohol (PVA) in the material. Additionally, the diffraction peak observed at  $39^\circ$  corresponds to the presence of iron pyrite ( $\text{FeS}_2$ ) in the material. JCPDS card # 79-0617 corresponds well with all the diffraction peaks.<sup>16</sup> In SERS, for the mechanism of charge transfer resonance to occur, the presence of oxygen vacancies and metallic sites in a material is highly preferred.<sup>17</sup>

Fig. 2(d) shows the FTIR spectra of  $\text{FeS}_2$  nanoflowers and  $\text{FeS}_2$  aerogel. The  $\text{FeS}_2$  nanoflowers showed transmittance peaks at  $\sim 2856, \sim 2376, \sim 1645, \sim 1176, \sim 809, \sim 613,$  and

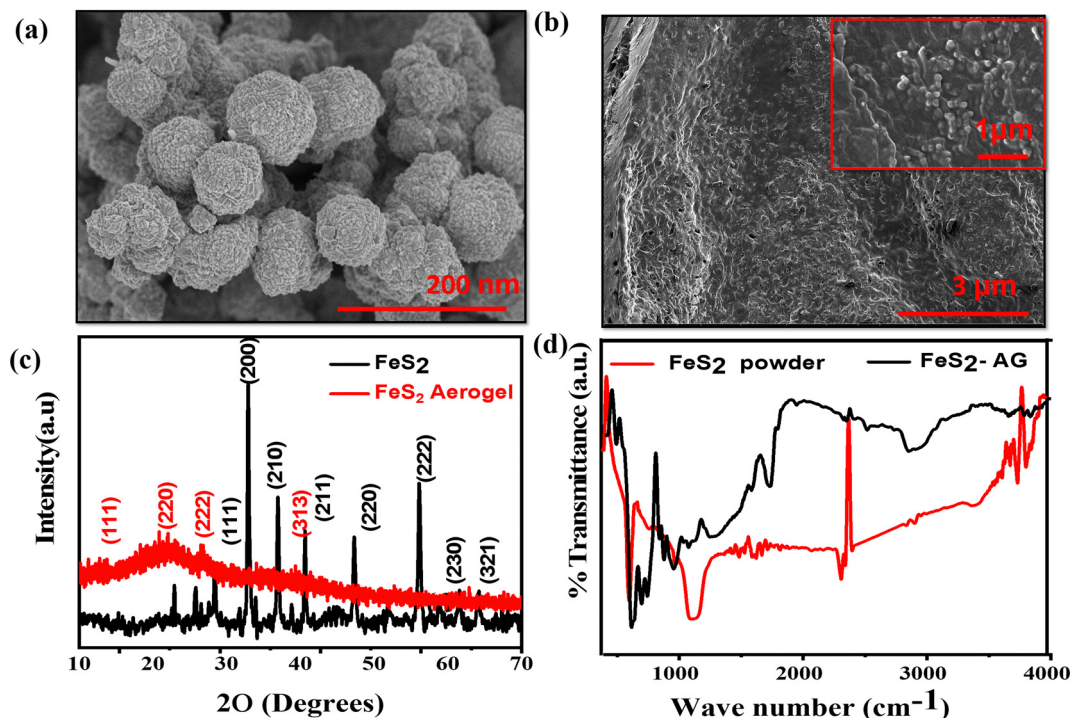


Fig. 2 (a) SEM image of FeS<sub>2</sub> nanoflowers and (b) low-magnification image of FeS<sub>2</sub> aerogel with the inset showing high magnification image of FeS<sub>2</sub> aerogel. (c) XRD patterns and (d) FTIR spectra of FeS<sub>2</sub> nanoflowers and FeS<sub>2</sub> aerogel.

$\sim 455\text{ cm}^{-1}$ . The peak at  $\sim 2856\text{ cm}^{-1}$  is ascribed to the C–H stretching vibration, while those at  $\sim 2376$ ,  $\sim 1645$ ,  $\sim 809$ , and  $\sim 613\text{ cm}^{-1}$  belong to O=C=O stretching, C=N stretching of imine, C–H bending and C–Fe stretching. The characteristic peak at  $\sim 1176\text{ cm}^{-1}$  is related to pyrite surface chemistry of FeS<sub>2</sub> nanoparticles<sup>18</sup> as is that at  $\sim 455\text{ cm}^{-1}$ . The FeS<sub>2</sub> aerogel spectrum almost coincided with that of FeS<sub>2</sub> nanoparticles. The transmittance peaks of the FeS<sub>2</sub> aerogel were observed at  $\sim 443$ ,  $\sim 624$ ,  $\sim 1115$ ,  $\sim 1589$ ,  $\sim 2397$ ,  $\sim 3415$ ,  $\sim 3800$ ,  $3756$ , and  $\sim 3796\text{ cm}^{-1}$ . The observed peak at  $1589\text{ cm}^{-1}$  is ascribed to the aromatic C=C group while the peak between  $3500$  and  $3700\text{ cm}^{-1}$  corresponds to the bending and stretching vibration of OH groups in water molecules which are adsorbed onto the surface of the aerogel. The peak observed at  $1050\text{ cm}^{-1}$  in the FTIR spectrum of the FeS<sub>2</sub> aerogel corresponds to the

vibrational frequency associated with the stretching mode of the C–O bond of the GO functional group. To obtain detailed information about the chemical structure, Raman spectroscopy was used and the details are explained in ESI†

### 3.2. Sensitivity study of FeS<sub>2</sub> aerogel SERS substrate

The standard probe molecule methylene blue (MB) is chosen for sensitivity study of the as-synthesised FeS<sub>2</sub> aerogel substrate. Fig. 3(a) illustrate SERS spectra of the FeS<sub>2</sub> aerogel substrate in the presence of MB concentrations from 50 to 500 nM. The concentration of MB spiked is proportional to the SERS peak intensity. High SERS intensity was observed for the characteristic peaks of MB even with the lowest concentration of 50 nM, which establishes the high sensitivity of FeS<sub>2</sub>-AG. The mechanism of

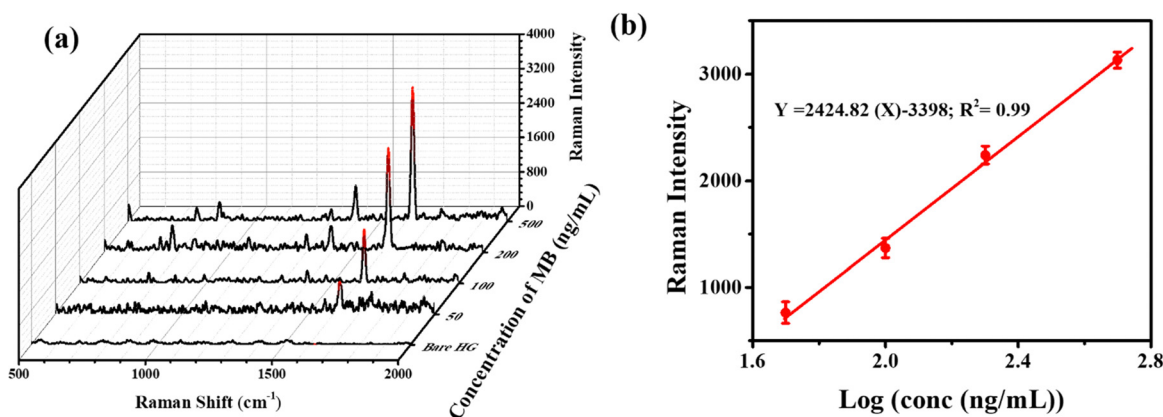


Fig. 3 (a) Sensitivity analysis of MB on FeS<sub>2</sub> aerogel. (b) Calibration plot for MB.



photoinduced charge transfer resonance caused by the laser-induced rapid charge transfer between the analyte molecules and the aerogel substrate is attributed as being responsible for the sensing ability of the as-fabricated sensor.

The characteristic peak of MB at  $\sim 1618\text{ cm}^{-1}$ , which is attributed to (C-C) ring stretching, indicates that the MB molecules have adsorbed well onto the aerogel substrate. Besides this, other characteristic peaks were observed at  $\sim 1399$ ,  $\sim 1249$ ,  $\sim 1274$ ,  $\sim 1036$  and  $\sim 948\text{ cm}^{-1}$  which were assigned to the stretching vibration of in-plane ring deformation of (C-H), (C-N), out-of-plane bending, in-plane bending and in-plane ring deformation of (C-H) respectively. Fig. 3(b) depicts the calibration plot with increasing concentration of MB. The linear regression equation for the detection of MB is  $Y = 2422.257(X) - 3392.536$  with an  $R^2$  of 0.994. The limit of detection (LOD) was calculated from the equation  $\text{LOD} = 3 s / m$ , where  $s$  is the standard deviation and  $m$  the slope of the linear calibration curve. For MB, the LOD was obtained as  $0.06\text{ ng mL}^{-1}$  with a sensitivity of  $2422.257\text{ ng mL}^{-1}$ .

### 3.3. SERS detection of histamine

The sensing of histamine using  $\text{FeS}_2\text{-AG}$  was studied as illustrated in Fig. 4(a) comparing the Raman and SERS spectra of bulk histamine with the same accumulation time. The fingerprint spectra of histamine consist of several characteristic peaks which correspond to different modes of vibrations as

shown in Table S1 of ESI.† Notably, histamine displayed weak signals owing to low Raman scattering, whereas with the  $\text{FeS}_2\text{-AG}$  substrate, a significant enhancement in SERS signal is observed.

A significant enhancement in the SERS spectrum is detected for the characteristic peak at  $1844\text{ cm}^{-1}$  which corresponds to the  $\nu(\text{C} \cong \text{N})$  stretching vibrations induced by a strong interaction between histamine and metallic sites of the  $\text{FeS}_2\text{-AG}$  substrate. The interaction between SERS substrate and histamine molecules leads to the reconstruction of the energy band-gap near to the photon energy of the excitation laser. The newly formed energy band leads to the occurrence of the Raman resonance effect, providing an enhancement in SERS signal over that of the Raman signal obtained from the bulk histamine.

Enhancement factor (EF) of the  $\text{FeS}_2\text{-AG}$  substrate for the detection of histamine can be calculated from eqn (1) as follows:

$$\text{EF} = (N_{\text{bulk}}/N_{\text{SERS}}) (I_{\text{SERS}}/I_{\text{bulk}}) \quad (1)$$

where  $I_{\text{SERS}}$  is the intensity of SERS spectra,  $I_{\text{bulk}}$  the Raman spectral intensity,  $N_{\text{SERS}}$  the number of surface adsorbed molecules, and  $N_{\text{bulk}}$  the molecule number in the laser illumination volume.

The  $N_{\text{SERS}}$  of the aerogel was calculated from eqn (2):

$$N_{\text{SERS}} = N_A \times (V \times C) \times 0.25 \pi \mu\text{m}^2 / (A) \quad (2)$$

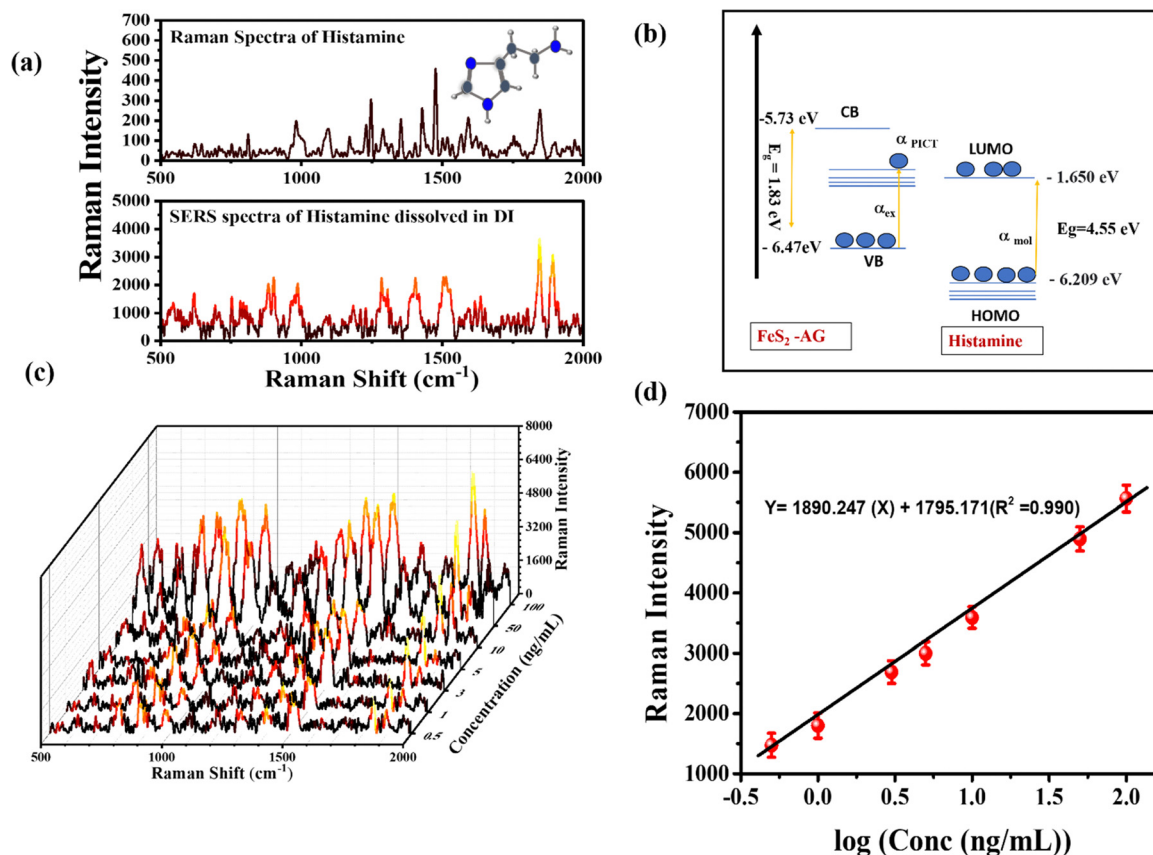


Fig. 4 (a) Raman and SERS spectra of histamine. (b) Band diagram showing charge transfer within  $\text{FeS}_2\text{-AG}$  and histamine. (c) SERS sensing of histamine. (d) Calibration curve for histamine.

where  $A$  is the effective surface area of the SERS substrate that is in contact with the sample,  $V$  the volume of histamine solution,  $N_A$  the numerical aperture of the lens used ( $\times 50$  LD, 0.9), and  $C$  the concentration of histamine. Thus, EF of the  $\text{FeS}_2$ -AG substrate was calculated as  $1.61 \times 10^7$  towards histamine.

This huge enhancement of SERS signal is attributed to the mechanism of charge transfer induced by the laser followed by the mechanism of photoinduced charge transfer (PICT) resonance.<sup>15,16</sup> The histamine molecules are adsorbed onto the substrate surface by surface CT complexes through weak covalent bonds.<sup>17</sup> Notably, the cubic structure of  $\text{FeS}_2$  provides numerous coordination sites of  $\text{Fe}^{2+}$  from the formation of anionic monomeric/dimeric sulphur vacancies at the interface region of the material.<sup>18</sup> As a consequence of this synergistic effect between generated oxygen vacancies *via* PICT resonance and the intrinsic deficiency of oxygen in the substrate, the interaction between histamine molecules and the substrate is enhanced.<sup>19</sup> Fig. 4(b) illustrates the mechanism of charge transfer between  $\text{FeS}_2$ -AG and histamine molecules. The conduction band (CB) of the  $\text{FeS}_2$ -AG substrate is located at  $-5.73$  eV with a valence band (VB) at  $-6.47$  eV.<sup>20</sup> Similarly, histamine molecules have a highest occupied molecular orbital (HOMO) at  $-6.209$  eV and a lowest unoccupied molecular orbital (LUMO) at  $-1.650$  eV.<sup>21</sup> The excitation of electrons of  $\text{FeS}_2$ -AG and histamine molecules leads to a notable enhancement in the SERS signal.

Fig. 4(c) depicts the SERS spectrum of histamine with an increasing concentration of histamine ( $0.5 \text{ ng mL}^{-1}$  to  $100 \text{ ng mL}^{-1}$ ). The observed peak at  $1844 \text{ cm}^{-1}$  is selected as the peak of interest due to it corresponding to the stretching vibration of carbon and nitrogen, not present for other interfering molecules, thus allowing the detection of histamine to be easy. The amplification of the peak observed at  $1844 \text{ cm}^{-1}$  with increasing histamine concentration substantiates the exceptional interaction between the substrate and analyte molecules. The calibration curve for histamine is depicted in Fig. 4(d). The linear regression equation for the detection of histamine is  $Y = 1890.247(X) - 1795.171$  with correlation coefficient ( $R^2$ ) of 0.990. The LOD of histamine was calculated from the previously

discussed equation as  $0.08 \text{ ng mL}^{-1}$  which highlights the suitability of the as-fabricated sensor for detecting physiological levels of histamine.

### 3.4. Selectivity and stability study

One major factor determining any biosensor's practicability is its selectivity. To determine the anti-interference ability and specificity of the sensor, data were taken in the presence of 2-fold concentration of interfering molecules like uric acid, urea, ascorbic acid, and glucose. Fig. 5 depicts peak intensities of the  $\text{FeS}_2$ -AG substrate containing  $50 \text{ ng mL}^{-1}$  of histamine with interfering molecules; however there was no significant changes noticed in the intensities of characteristic peaks. This outstanding performance obtained for selectivity of  $\text{FeS}_2$ -AG was accredited to the interaction of histamine molecules and the substrate *via* the presence of  $\nu(\text{C} \cong \text{N})$  stretching vibrations that are unique for histamine.

This same  $\text{FeS}_2$ -AG sensor was utilised for stability studies for detection of histamine molecules. The SERS spectrum was measured every 5 consecutive days (data not shown). It was found that the peak intensity at  $1844 \text{ cm}^{-1}$  corresponding to histamine declines at a negligible rate. Thus, it is clear that the substrate possesses excellent chemical stability. The SERS spectrum of histamine was measured from 110 different positions to check the reliability of the measurements. Here, a noticeable change in intensities of the peaks was observed; however, it is below 10% relative standard deviation. This demonstrates the remarkable homogeneousness of the histamine-adsorbing  $\text{FeS}_2$ -AG substrate.

Table 1 compares the performance of  $\text{FeS}_2$ -AG as SERS substrate with earlier reported substrates for the detection of histamine. Many researchers have used composite materials with expensive plasmonic metals which limits their practical applications.<sup>22–26</sup> One of the main concerns regarding the fabrication of SERS-active substrates is the possible overlapping of the substrate signal with the analyte signal. In this work,  $\text{FeS}_2$  was used in qualitative analytical techniques for detection of histamine which showed minimal to no interference with the histamine signal. It should be highlighted that low binding

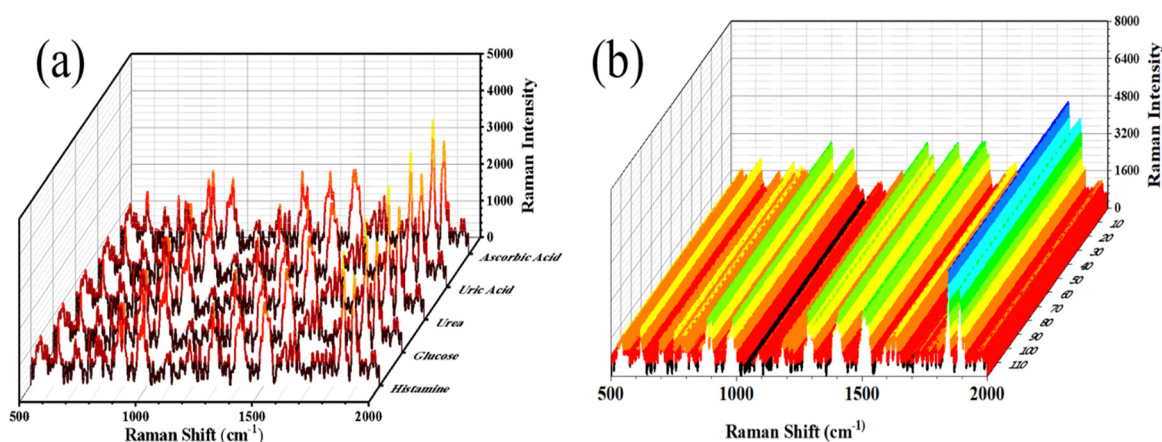


Fig. 5 (a) SERS spectra of histamine with mutual interference. (b) SERS spectra of histamine at different concentrations.

**Table 1** Performance comparison of the as-fabricated FeS<sub>2</sub>-AG SERS substrate towards detection of histamine with other reported SERS sensors

No.	Substrate used	Flexible	Real time sample	Linear range	LOD	Ref.
1	Au-NTA-Ni(II)	No	Serum	1 to 50 $\mu\text{M}$	1 $\mu\text{M}$	7
2	SiO <sub>2</sub> AuAg	No	Fish	0.1 to 0.8 mM	3.697 ppm	24
3	Fe <sub>3</sub> O <sub>4</sub> /AuATPAG	No	Fish	10 <sup>-8</sup> to 10 <sup>-3</sup> M	20 mg kg <sup>-1</sup>	25
4	AgNPs + MIPs	No	Food samples	0.1 to 100 mg L <sup>-1</sup>	0.040 mg L <sup>-1</sup>	27
5	Silver nanoparticles	No	Fish	0 to 200 mg L <sup>-1</sup>	10 mg L <sup>-1</sup>	28
6	FeS <sub>2</sub> -AG	Yes	Serum	0.5 to 100 ng mL <sup>-1</sup>	0.08 ng mL <sup>-1</sup>	This work

ATP, aminothiophenol; NTA, nitrilotriacetic acid; MIP, molecularly imprinted polymers.

affinities of biomolecules with metallic nanostructures make it difficult to obtain high-quality SERS spectra from biomolecules.<sup>23</sup>

This work represents a simple low-cost detection of histamine in blood using SERS analysis, while others reported quantification and detection of histamine from food samples.<sup>22,24</sup> Besides, the selectivity of the FeS<sub>2</sub>-AG substrate in the presence of interfering molecules was appreciably good, thus highlighting its efficiency as a promising platform for bioanalytical applications.

## 4. Conclusion

Herein, we demonstrate a cubic-structured FeS<sub>2</sub> nanoflower-based aerogel as a flexible and low-cost substrate for SERS detection of histamine in blood. This as-fabricated sensor demonstrated exceptional selectivity towards histamine molecules with an EF of  $1.61 \times 10^7$  and high stability with a low LOD value of 0.08 ng mL<sup>-1</sup> which make the as-fabricated sensor suitable for clinical applications. Moreover, the FeS<sub>2</sub>-AG substrate was found to be successful in detecting histamine from samples of simulated blood serum with an excellent value of recovery percentage. The overall efficiency of the FeS<sub>2</sub>-AG substrate towards histamine sensing proves it as a functional platform for diverse bioanalytical applications. With the combination of this sensor with an electrochemical potentiostat and smartphone, a personal health monitoring system can be developed to diagnose histamine intolerance and food poisoning in the future.

## Author contributions

Anjali Sreekumar – methodology, data curation, validation, visualization, writing – original draft preparation. Lignesh Durai – methodology, data curation, validation, visualization. Minu Thomas – methodology, data curation, validation. Sushmee Badhulika – conceptualization, funding acquisition, investigation, project administration, resources, supervision, writing – review & editing.

## Conflicts of interest

The authors have no competing interests.

## Acknowledgements

S. B. acknowledges financial assistance from Department of Science and Technology (DST) Nano Mission project DST/NM/NT/2020/322.

## References

- X. Peng, L. Yang, Z. Liu, S. Lou, S. Mei, M. Li, Z. Chen and H. Zhang, *Nat. Commun.*, 2022, **13**(1), 1–9.
- M. Gagic, E. Jamroz, S. Krizkova, V. Milosavljevic, P. Kopel and V. Adam, *J. Agric. Food Chem.*, 2018, **67**(3), 773–783.
- Y. Zhao, X. Zhang, H. Jin, L. Chen, J. Ji and Z. Zhang, *Biomolecules*, 2022, **12**(3), 454.
- H. J. Zhang, W. Y. Chen, X. Zou, Q. Sun and E. Q. Gao, *J. Electrochem. Soc.*, 2022, **169**(7), 077511.
- L. Lu, Y. Zhou, T. Zheng and Y. Tian, *Nano Res.*, 2022, 1–6.
- I. B. Ansah, W. C. Lee, C. Mun, J. J. Rha, H. S. Jung, M. Kang, S. G. Park and D. H. Kim, *Sens. Actuators, B*, 2022, **353**, 131196.
- P. Li, B. Zhou, M. Ge, X. Jing and L. Yang, *Talanta*, 2022, **237**, 122913.
- L. Durai and S. Badhulika, *Microchim. Acta*, 2021, **188**, 1–9.
- L. Tang, S. Li, F. Han, L. Liu, L. Xu, W. Ma, H. Kuang, A. Li, L. Wang and C. Xu, *Biosens. Bioelectron.*, 2015, **71**, 7–12.
- A. Bolotsky, D. Butler, C. Dong, K. Gerace, N. R. Glavin, C. Muratore, J. A. Robinson and A. Ebrahimi, *ACS Nano*, 2019, **13**(9), 9781–9810.
- R. T. Lowson, *Chem. Rev.*, 1982, **82**(5), 461–497.
- A. P. Chandra and A. R. Gerson, *Surf. Sci. Rep.*, 2010, **65**(9), 293–315.
- S. Huh, J. Park, Y. S. Kim, K. S. Kim, B. H. Hong and J. M. Nam, *ACS Nano*, 2011, **5**(12), 9799–9806.
- A. K. Haridas, M. K. Sadan, Y. Liu, H. Y. Jung, Y. Lee, H. J. Ahn and J. H. Ahn, *J. Alloys Compd.*, 2022, **928**, 167125.
- L. Durai and S. Badhulika, *Adv. Mater. Interfaces.*, 2022, **9**(13), 2200146.
- J. X. Hu, Q. Li, H. L. Zhu, Z. N. Gao, Q. Zhang, T. Liu and G. M. Wang, *Nat. Commun.*, 2022, **13**(1), 1–9.
- J. Yu, C. Chen, J. Lin, X. Meng, L. Qiu and X. Wang, *J. Mater. Chem. C*, 2022, **10**(5), 1632–1637.
- M. A. L. I. H. E. H. Khabbaz and M. H. Entezari, *J. Colloid Interface Sci.*, 2016, **470**, 204–210.
- S. Aftab, M. Z. Iqbal and M. W. Iqbal, *Adv. Mater. Interfaces*, 2022, 2201219.
- R. Sha, N. Vishnu and S. Badhulika, *IEEE Trans. Nanotechnol.*, 2022, **21**, 374–379.
- L. Durai and S. Badhulika, *Ceram. Int.*, 2022, **48**(13), 18667–18675.
- M. Zebarjad, F. Jamali-Sheini and R. Yousefi, *Ceram. Int.*, 2023, **49**(1), 323–334.
- C. Zong, M. Xu, L. J. Xu, T. Wei, X. Ma, X. S. Zheng, R. Hu and B. Ren, *Chem. Rev.*, 2018, **118**(10), 4946–4980.

- 24 K. H. Huynh, X. H. Pham, E. Hahm, J. An, H. M. Kim, A. Jo, B. Seong, Y. H. Kim, B. S. Son, J. Kim and W. Y. Rho, *Int. J. Mol. Sci.*, 2020, **21**(11), 4048.
- 25 T. Zhou, M. Fan, R. You, Y. Lu, L. Huang, Y. Xu, S. Feng, Y. Wu, H. Shen and L. Zhu, *Anal. Chim. Acta*, 2020, **1104**, 199–206.
- 26 P. Li, B. Zhou, M. Ge, X. Jing and L. Yang, *Talanta*, 2022, **237**, 122913.
- 27 Z. Wu, E. Xu, A. Jiao, Z. Jin and J. Irudayaraj, *RSC Adv.*, 2017, **7**(71), 44933–44944.
- 28 T. Janči, D. Valinger, J. G. Kljusurić, L. Mikac, S. Vidaček and M. Ivanda, *Food Chem.*, 2017, **224**, 48–54.